LETTER

doi:10.1038/nature12588

Vinylogous chain branching catalysed by a dedicated polyketide synthase module

Tom Bretschneider[1], Joel B. Heim[2], Daniel Heine[1], Robert Winkler[1], Benjamin Busch[1], Björn Kusebauch[1], Thilo Stehle[2,3], Georg Zocher[2] & Christian Hertweck[1,4]

Bacteria use modular polyketide synthases (PKSs) to assemble complex polyketides, many of which are leads for the development of clinical drugs, in particular anti-infectives and anti-tumoral agents[1]. Because these multifarious compounds are notoriously difficult to synthesize, they are usually produced by microbial fermentation. During the past two decades, an impressive body of knowledge on modular PKSs[2,3] has been gathered that not only provides detailed insight into the biosynthetic pathways but also allows the rational engineering of enzymatic processing lines to yield structural analogues[4,5]. Notably, a hallmark of all PKS modules studied so far is the head-to-tail fusion of acyl and malonyl building blocks, which leads to linear backbones. Yet, structural diversity is limited by this uniform assembly mode. Here we demonstrate a new type of PKS module from the endofungal bacterium *Burkholderia rhizoxinica* that catalyses a Michael-type acetyl addition to generate a branch in the carbon chain. *In vitro* reconstitution of the entire PKS module, X-ray structures of a ketosynthase-branching didomain and mutagenesis experiments revealed a crucial role of the ketosynthase domain in branching the carbon chain. We present a trapped intermediary state in which acyl carrier protein and ketosynthase are covalently linked by the branched polyketide and suggest a new mechanism for chain alkylation, which is functionally distinct from terpenoid-like β-branching. For the rice seedling blight toxin rhizoxin, one of the strongest known anti-mitotic agents, the non-canonical polyketide modification is indispensable for phytotoxic and anti-tumoral activities. We propose that the formation of related pharmacophoric groups follows the same general scheme and infer a unifying vinylogous branching reaction for PKS modules with a ketosynthase-branching–acyl-carrier-protein architecture. This study unveils the structure and function of a new PKS module that broadens the biosynthetic scope of polyketide biosynthesis and sets the stage for rationally creating structural diversity.

In light of the highly diverse architectures of polyketide metabolites, it is surprising to learn that their carbon backbones are produced by rather basic enzymatic mechanisms that are reminiscent of fatty acid biosynthesis[6,7]. The minimal requirement is an acyl carrier protein (ACP) that serves as an anchor for the growing chain, an acyl transferase (AT) that loads activated malonyl building blocks onto the ACP and a ketosynthase (KS) that catalyses the head-to-tail carbon bond formation between the malonyl and acyl units tethered to the KS and ACP. Ketoreductase, dehydratase and enoyl reductase domains may optionally be involved in processing the β-keto group that results from the KS-mediated Claisen condensation[6]. Apart from the number of chain propagations and the degree of β-keto processing, alkyl side chains largely contribute to polyketide diversity. Alkyl substituents at α-positions to a former carbonyl residue may result from the incorporation of substituted malonyl units or α-methylation[8]. Furthermore, terpenoid-like alkylations at β-positions have been observed in various polyketide pathways, in which a set of freestanding enzymes act *in trans* to modify the β-keto group in analogy to mevalonate biosynthesis[9] (Fig. 1c).

Such polyketide chain branches may play a key part in the biological activity of polyketides. A particularly noteworthy example is rhizoxin (**1b**), the phytotoxin produced in a rare fungal–bacterial symbiosis of the rice seedling blight fungus *Rhizopus microsporus* and its endofungal bacterium *B. rhizoxinica*[10,11]. Owing to its efficient binding to β-tubulin subunits, rhizoxin congeners represent some of the strongest anti-mitotic agents known and are considered as promising anti-tumoral agents[12]. Yet, structure–activity relationships and modelling studies have revealed that the anti-mitotic activity of the molecule crucially depends on the short (C2) carbon chain that branches off from the macrolide ring at C6 (refs 13–15). The formation of this pharmacophoric residue could not be rationalized by any biosynthetic precedence as genes for terpenoid-like β-alkylation were absent in the bacterial genome[16,17]. Analysis of the gene cluster coding for the rhizoxin D1 (**1a**) polyketide synthase[18] (Fig. 1a and Supplementary Fig. 1) and structural elucidation of prematurely released pathway intermediates strongly suggested that the β-branch is introduced by a Michael addition of a C2 unit to an α,β-unsaturated thioester[19] (Fig. 1b).

Bioinformatic analyses and *in vivo* dissection of the rhizoxin pathway indicated that an unusual PKS module located on RhiE would have a role in the chain-branching event[19]. The designated module consists of a typical KS domain, an ACP domain and a cryptic branching ('B') domain in between, which does not show any homology to known enzyme domains. To determine the essential components for polyketide chain branching and to gain insight into the reaction mechanism, we fully reconstituted the PKS module *in vitro*. Reaching this goal was challenging because it afforded a variety of pure, functional and, in part, post-translationally modified proteins as well as the appropriate substrates (Fig. 2A and Supplementary Information). In short, we heterologously produced tagged ketosynthase-branching (KS-B) didomain (RhiE$^{\#}$) of the branching module, the requisite ACP from the same module (Fig. 2B), which was transformed into its *holo* form by an endogenous phosphopantetheine transferase (PPTase) encoded in the *B. rhizoxinica* genome[17] (Fig. 2C), and the *trans*-acting AT (RhiG) for loading malonyl units onto the ACP. The module was split into KS-B and ACP domains to allow for flexible substrate loading and for analysis of ACP-bound products. To provide a substrate for the enzyme assay, we synthesized *N*-acetylcysteamine (SNAC) thioester **2**, a truncated surrogate of the polyketide intermediate produced upstream of the branching module. The enzymatic chain branching reaction was performed *in vitro* by mixing the His-tagged KS-B didomain (His-KS-B), His-tagged *holo*-ACP (His-ACP), His-tagged AT (AT-His), malonyl-CoA, and the synthetic surrogate substrate **2**. By matrix-assisted laser desorption/ionization–time of flight (MALDI–TOF) analysis of the ACP adduct (**3**) we detected a new compound attached to the ACP with the expected molecular mass. Product formation was confirmed by liquid chromatography–mass spectrometry (LC–MS) analysis of the product (Fig. 2D) liberated by the PPant ejection method[20]. To confirm unequivocally the identity of the lactone (**4**), we synthesized a synthetic

[1]Department of Biomolecular Chemistry, Leibniz Institute for Natural Product Research and Infection Biology (HKI), Jena 07745, Germany. [2]Interfaculty Institute of Biochemistry, Eberhard Karls University Tübingen, Tübingen 72076, Germany. [3]Department of Pediatrics, Vanderbilt University School of Medicine, Nashville, Tennessee 37232, USA. [4]Chair for Natural Product Chemistry, Friedrich Schiller University, Jena 07737, Germany.

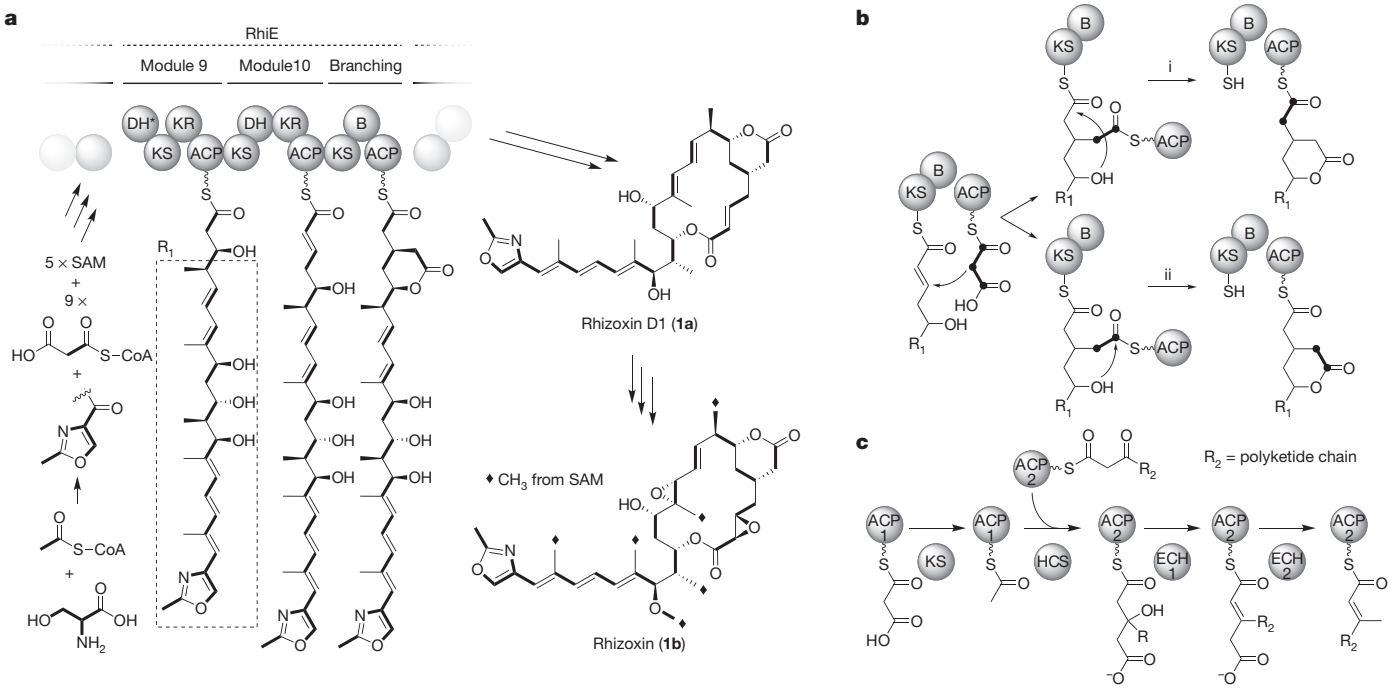

Figure 1 | Model of rhizoxin biosynthesis and chain branching mechanisms. a, Type I PKS for assembly of the rhizoxin backbone and structure of rhizoxin D1 (**1a**) (the box designates residue R_1 in **b**). ACP, acyl carrier protein; AT, acyl transferase; B, branching domain; DH, dehydratase; KR, ketoreductase; KS, ketosynthase. **b**, Possible course of chain-branching reaction highlighting two different lactonization routes. **c**, Isoprenoid-like β-branching reaction catalysed by *trans*-acting enzymes. ECH, enoyl-CoA hydratase/crotonase; HCS, 3-hydroxy-3-methylglutaryl-CoA (HMG-CoA) synthase.

reference and compared it with the hydrolysed enzyme product (**4**) by high-resolution LC–MS (HRMS). Notably, the enzyme reaction performed with heat-inactivated His-KS-B did not yield any product (Fig. 2E), thus proving the catalytic activity of the PKS module.

To gain deeper insight into this unusual reaction we studied the structure of the non-canonical PKS module. For improved protein stability we generated a truncated version of His-KS-B (RhiE*), which crystallized and led to a structural model of the KS-B module at 2.14 Å resolution (Fig. 3 and Supplementary Table 1). The KS-B module is a dimeric protein and folds into three domains (Fig. 3a and Supplementary Fig. 3). The KS domain shows a typical thiolase fold[21] and is flanked by a small linker region. A long linker runs across the entire KS-B RhiE module (Fig. 3a) and connects the *N*-terminal domains with the B domain. The B domain itself shares no noteworthy sequence homology (sequence identity is below 15%) to any known PKS domains described so far, but features a double hot dog (DHD) fold that is present in dehydratase domains[22]. A structural comparison (Supplementary Fig. 4) revealed highest structural homology to the product template domain (dehydratase-fold domain) of a fungal PKS[23] (Supplementary Table 2).

Binding of the substrate mimic **2** to the KS was confirmed by LC–MS. Moreover, X-ray crystallography revealed positive electron density in one chain next to the catalytic cysteine of the active site of the KS (Fig. 3c), thus suggesting that the KS domain is involved in the branching reaction.

To clarify the role of the KS domain in the branching reaction we intended to study the KS domain as a standalone enzyme. However, despite various efforts it was not possible to obtain a catalytically active KS domain outside the module. Thus, as an alternative, we inspected the active site of the KS domain and generated point mutations of the catalytic triad (Cys-His-His) in the intact KS-B didomain (Supplementary Fig. 5). Specifically, we replaced the cysteine with serine and alanine, and mutated each of the two histidines into alanine. Notably, none of the mutants showed any chain branching activity in the established assay. This finding provided clear evidence that the intact active site of the KS is crucial for the β-branching reaction.

Next, we investigated the role of the B domain in chain branching. We noted that the histidine-aspartate dyad, a hallmark of typical dehydratase domains, is altered in the B domain of RhiE. Notably, point mutation of the conserved aspartate residue amino acid in the B domain (Asp3876Ala mutant) did not affect the branching activity. Furthermore, we heterologously produced a freestanding, soluble B domain. In the absence of the KS domain, however, no branching activity was observed, indicating that this domain alone is not sufficient to catalyse the Michael addition.

There are several possible routes to the enzyme-mediated course of the vinylogous attack and lactone formation. In principle, the δ-lactone ring could be formed by installing the C–C bond before esterification, or vice versa. Furthermore, in the more likely case of an initial C–C bond formation, the δ-hydroxyl group (at C5) of the thioester intermediate could potentially attack the C1 carbonyl bound to the KS (Fig. 1b, route i) or the carbonyl of the added malonyl unit bound to the ACP (Fig. 1b, route ii). The course of the reaction has implications for the resulting polyketide chain because the C2 unit introduced by the branching module would be found in either the polyketide backbone or the side chain.

To solve this riddle we performed stable isotope labelling experiments *in vitro*. After addition of ^{13}C-labelled malonyl-CoA to the enzyme mixture and the synthetic surrogate, the product (**4**) was analysed by HRMS. MS/MS fragmentation, however, did not reveal the site of isotope incorporation (**4**) because fragments with the same molecular formula can arise from different parts of the symmetric substructure. To overcome this limitation we pursued an NMR analysis of the labelled reaction product still tethered to the entire ACP domain. After performing the enzyme assay, the ACP domain was purified and subjected to NMR measurements. By this approach we observed two strong NMR signals that correspond to the C1 and C2 positions of the thioester bound to the ACP (Fig. 4a). To confirm unequivocally the structure of the ACP-bound product, we synthesized the corresponding SNAC thioester and verified the identity of the chemical shifts. Consequently, the carbons of the malonyl unit added by the branching module are found in the linear polyketide chain, whereas the C1 and C2 carbons of the precursor molecule constitute the side chain (Fig. 4a).

This reaction scheme is quite intriguing as it suggests an unprecedented model in which a polyketide intermediate would be covalently tethered to both the KS and the ACP (Fig. 4b). To test this model we

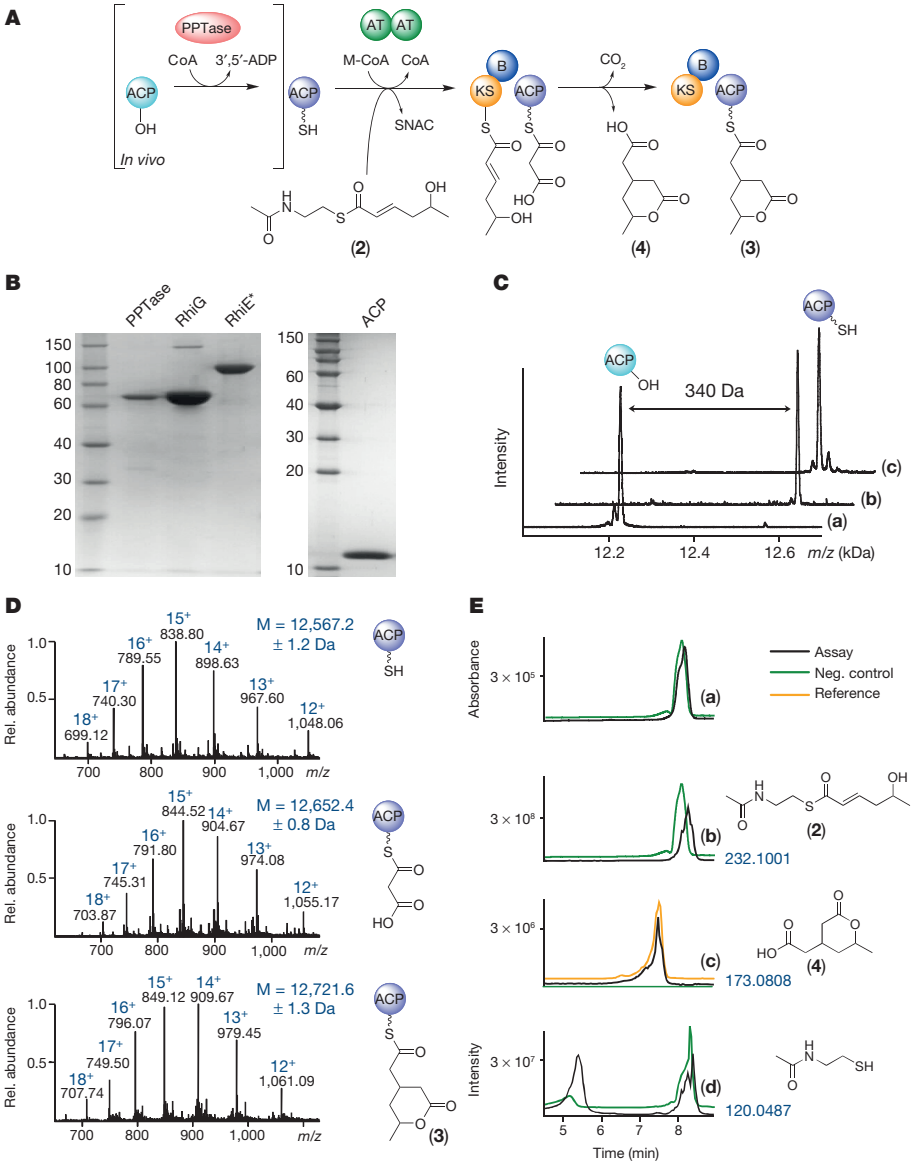

Figure 2 | *In vitro* reconstitution of the chain branching reaction. **A**, General experimental set-up for *in vitro* analysis of enzyme functions. **B**, Recombinant MalE-PPTase (70.7 kilodaltons (kDa)), RhiG-His (75.9 kDa, dimer at 152 kDa) and His-RhiE* (104.7 kDa) on a 10% SDS gel; His-ACP (12.2 kDa) on a 15% SDS gel. **C**, MALDI mass spectrum of *apo*-ACP (**a**) and *holo*-ACP, phosphopantetheinylated (wavy line) *in vitro* (**b**) and *in vivo* (**c**), indicated by mass shift (340 Da). **D**, Analysis of ACP species by LC–MS. Rel., relative. **E**, LC–HRMS analysis of enzymatic chain branching. HPLC trace ($UV_{220\,nm}$) (**a**), and extracted *m/z* chromatograms of 232.1001 (**2**) (**b**), 173.0808 (**4**) (**c**), and 120.0487 (liberated *N*-acetylcysteamine) (**d**). Retention times of diasteromers of **4** are identical. Neg., negative.

designed an experiment that allows trapping the proposed intermediary state. We reasoned that a substrate analogue lacking the hydroxyl moiety (**5**) would still undergo the Michael addition of the ACP-bound nucleophile, but the subsequent lactonization of the thioester would be prevented. For this purpose we synthesized the deoxy variant (**5**) and performed the multi-enzyme assay as described above. SDS-gel electrophoresis of the reaction mixture revealed a band that corresponds to the size of KS-B and ACP. Notably, this band is absent in an assay using **2**, where only the band for KS-B can be detected (Fig. 4c). Analysis of this band by tryptic mass fingerprinting revealed the presence of the ACP in the top band, whereas it was missing in the bottom band and the negative control (Supplementary Fig. 7). We repeated this assay with the point-mutated KS mutants and found that protein cross-linking does not take place in the Cys3227Ala, Cys3227Ser and His3404Ala KS mutants, once again confirming the crucial role of a catalytically intact KS domain. It is interesting to note that the His3364Ala mutant retains weak activity for vinylogous addition using deoxy variant **5**, whereas it cannot catalyse lactonization when surrogate **2** is used (see above). Taken together, the KS clearly has a key role in forming an enolate for the vinylogous addition to the unsaturated thioester. Chain propagation is only possible by lactonization involving the δ-hydroxy group of the resulting intermediate and the C1 carbonyl, and C1 and C2 of the former linear chain constitute the side chain. It is generally conceivable that the unusual B domain assists in the formation of the δ-lactone ring. However, an interaction of the B domain with the KS-ACP-linked intermediate is rather unlikely given the large distance between the active site cavities of the KS and B domains (Fig. 3). Because mutation of the conserved Asp residue resulted in an enzyme species that is still able to catalyse the vinylogous branching reaction, one may conclude that the B domain seems to have a rather structural role in the module.

A vast number of modular PKS systems have been investigated at the molecular and biochemical levels. Yet, in all studied examples PKS modules catalyse the head-to-tail fusion of acyl and malonyl units, thus invariably yielding a linear polyketide chain[6]. Our results show, for the first time, direct evidence for a vinylogous addition of a malonyl building block to a polyketide chain, which results in chain branching (Fig. 4b). This non-canonical branching reaction is catalysed by a novel type of module consisting of KS, B and ACP domains, as shown by the successful *in vitro* reconstitution of the entire module and transformation of a substrate mimic. As a proof of concept, we used NMR analysis of an ACP-bound, branched reaction product to complement mass spectrometry and MALDI analyses. The results reported here will have broad implications for the field of polyketide biosynthesis. First, we unveil a novel role for a ketosynthase in polyketide biosynthesis[24,25]. As point mutations and the chemical cross-linking reaction revealed, a catalytically active KS domain is indispensable for the vinylogous

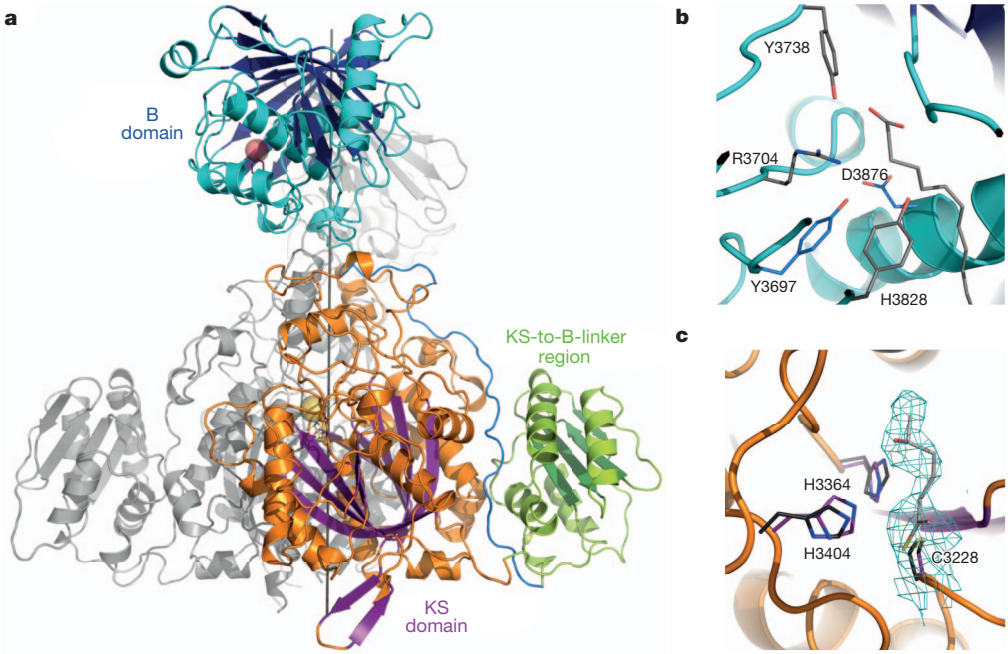

Figure 3 | Domain structures of branching module (RhiE*). **a**, Overall structure of the dimeric RhiE module, coloured by its domain organization. Two-fold axis is indicated by a black line. Domain active sites are highlighted by yellow (KS) and red (B) spheres. **b**, Active centre of KS domain in superposition to its structural most related protein (PDB code 2HG4). Unbiased electron density ($2F_o - F_c$) shown at a contour level of 1.0 in cyan. The substrate was modelled into the cavity on the basis of electron density (not included in coordinates of RhiE). **c**, Comparison of the active site of the B domain with a dehydratase domain of 6-deoxyerythonolide B synthase (PDB code 3HRR).

addition of the malonyl unit. In light of the countless known KS domains that uniformly produce linear carbon chains, our finding is a showcase for a substantially different KS-mediated reaction channel. It should also be highlighted that the crystal structure of the KS-B didomain features the first structure of a KS domain from the growing class of *trans*-AT modular PKS[26]. We reason that the three-dimensional structural data provide new structural insight into the functioning of these important assembly lines. Notably, homologues of the KS-B didomains are encoded in gene clusters for the biosynthesis of various antibiotics featuring cycloheximide-like glutarimide substructures, such as migrastatin[27] and 9-methylstreptimidone[28], in which vinylogous additions by amides (in lieu of hydroxyl) have been suggested but not experimentally proven.

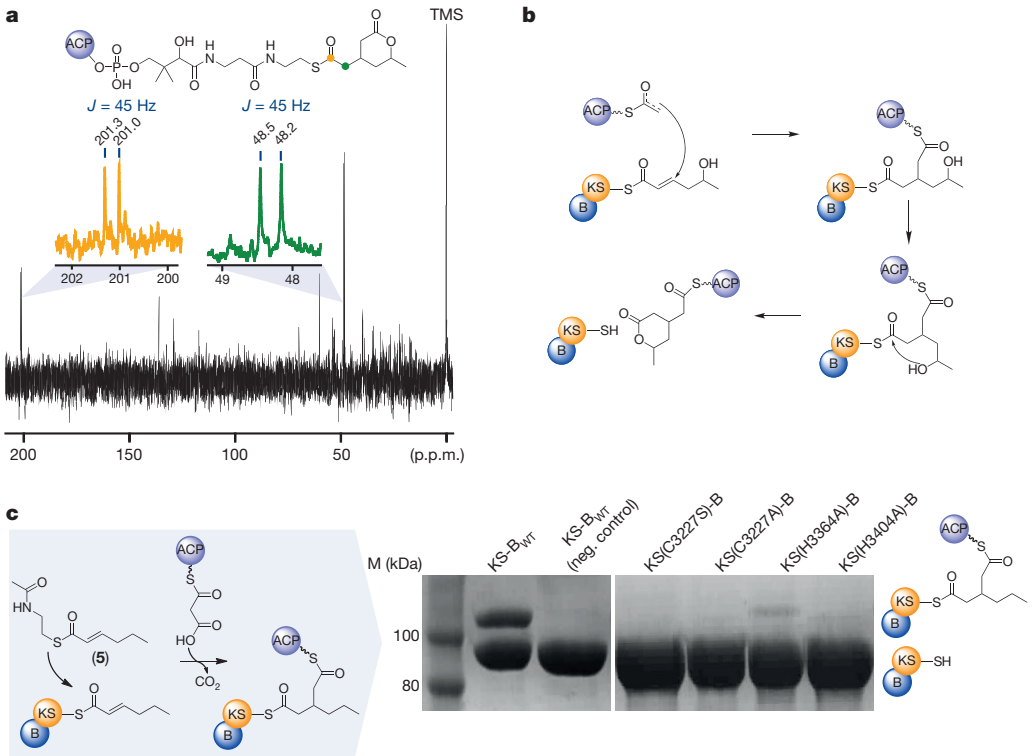

Figure 4 | Model of enzyme mechanism for Michael addition and lactone formation based on NMR and SDS–PAGE analyses. **a**, NMR spectrum of the ^{13}C-labelled product (derived from ^{13}C-labelled malonate) still tethered to the ACP. TMS, tetramethylsilane. **b**, SDS–PAGE analysis of the chain branching-assay using deoxy analogue **5**, trapping the intermediary covalent adduct between the KS-B and the ACP domains, which results in a band shift. (For gel-band analysis by tryptic fingerprinting see Supplementary Information.) In addition to the wild-type KS, the reaction was repeated using several KS mutants. In the assay using substrate mimic **2** the adduct forms only transiently and cannot be visualized on the gel (negative control). **c**, Model of the chain branching reaction inferred from experimental data.

We propose that the mechanism for glutarimide formation in these and related pathways follows the same general scheme unveiled in this study and infer a unifying mechanism for chain vinylogous branching in PKS modules with a KS-B-ACP architecture. Undoubtedly, polyketide chain branching represents a means to expand the structural space of polyketide metabolites. Because the δ-lactone moiety in rhizoxin[13] and the glutarimide substructures in cycloheximide-type antibiotics[29] represent crucial pharmacophoric residues, it is interesting to learn that functionally divergent KS domains have evolved in modular PKS to grant access to these non-canonical traits. The branching module is an important addition to the enzymatic toolbox of polyketide synthases. It is conceivable that this unusual module could be implanted into other modular PKS to expand the range of naturally polyketide metabolites and to generate analogues of therapeutics that are not readily accessible by synthetic methods. Our findings not only illustrate a novel enzymatic modification that broadens the scope of modular assembly lines, but also create new opportunities for rationally engineering novel polyketide structures.

METHODS SUMMARY

All recombinant protein species were heterologously expressed in *Escherichia coli* and subsequently purified in a two-step approach by using affinity and anion exchange chromatography. The protein purity and identity were confirmed by MALDI–TOF/TOF (UltrafleXtreme, Bruker). The pure protein species were used for *in vitro* reconstruction of the enzymatic reaction by co-incubation with synthetic substrate surrogates. Their authenticity was confirmed by NMR (Bruker Avance III with cryo probe) as well as the synthetic reference compounds. The resultant ACP species were analysed by MALDI and liquid chromatography/electrospray ionization mass spectrometry (LC-ESI-MS) (LTQ, ThermoFisher). The RhiE* protein was crystallized by sitting drop vapour diffusion, and its structure was determined by molecular replacement.

Full methods for the protein production, assays, protein structure analysis, mutant construction, detailed synthetic procedures and physicochemical characterization of new compounds including NMR are available in the Methods.

Online Content Any additional Methods, Extended Data display items and Source Data are available in the online version of the paper; references unique to these sections appear only in the online paper.

Received 15 May; accepted 19 August 2013.
Published online 18 September 2013.

1. Fischbach, M. A. & Walsh, C. T. Assembly-line enzymology for polyketide and nonribosomal peptide antibiotics: logic, machinery, and mechanisms. *Chem. Rev.* **106,** 3468–3496 (2006).
2. Khosla, C., Kapur, S. & Cane, D. E. Revisiting the modularity of modular polyketide synthases. *Curr. Opin. Chem. Biol.* **13,** 135–143 (2009).
3. Keatinge-Clay, A. T. The structures of type I polyketide synthases. *Nat. Prod. Rep.* **29,** 1050–1073 (2012).
4. Weissman, K. J. & Leadlay, P. F. Combinatorial biosynthesis of reduced polyketides. *Nature Rev. Microbiol.* **3,** 925–936 (2005).
5. Wong, F. T. & Khosla, C. Combinatorial biosynthesis of polyketides–a perspective. *Curr. Opin. Chem. Biol.* **16,** 117–123 (2012).
6. Hertweck, C. The biosynthetic logic of polyketide diversity. *Angew. Chem. Int. Ed. Engl.* **48,** 4688–4716 (2009).
7. Khosla, C. Structures and mechanisms of polyketide synthases. *J. Org. Chem.* **74,** 6416–6420 (2009).
8. Wilson, M. C. & Moore, B. S. Beyond ethylmalonyl-CoA: the functional role of crotonyl-CoA carboxylase/reductase homologs in expanding polyketide diversity. *Nat. Prod. Rep.* **29,** 72–86 (2012).
9. Calderone, C. T. Isoprenoid-like alkylations in polyketide biosynthesis. *Nat. Prod. Rep.* **25,** 845–853 (2008).
10. Partida-Martinez, L. P. & Hertweck, C. Pathogenic fungus harbours endosymbiotic bacteria for toxin production. *Nature* **437,** 884–888 (2005).
11. Scherlach, K., Busch, B., Lackner, G., Paszkowski, U. & Hertweck, C. Symbiotic cooperation in the biosynthesis of a phytotoxin. *Angew. Chem. Int. Ed. Engl.* **51,** 9615–9618 (2012).
12. Scherlach, K., Partida-Martinez, L. P., Dahse, H.-M. & Hertweck, C. Antimitotic rhizoxin derivatives from cultured symbionts of the rice pathogenic fungus *Rhizopus microsporus*. *J. Am. Chem. Soc.* **128,** 11529–11536 (2006).
13. Hong, J. & White, J. D. The chemistry and biology of rhizoxins, novel antitumor macrolides from *Rhizopus chinensis*. *Tetrahedron* **60,** 5653–5681 (2004).
14. Schmitt, I. *et al.* Evolution of host-resistance in a toxin-producing fungal-bacterial mutualism. *ISME J.* **2,** 632–641 (2008).
15. Kusebauch, B., Scherlach, K., Kirchner, H., Dahse, H. M. & Hertweck, C. Antiproliferative effects of ester- and amide-functionalized rhizoxin derivatives. *ChemMedChem* **6,** 1998–2001 (2011).
16. Lackner, G., Moebius, N., Partida-Martinez, L. P. & Hertweck, C. Complete genome sequence of *Burkholderia rhizoxinica*, an Endosymbiont of *Rhizopus microsporus*. *J. Bacteriol.* **193,** 783–784 (2011).
17. Lackner, G., Moebius, N., Partida-Martinez, L. P., Boland, S. & Hertweck, C. Evolution of an endofungal lifestyle: deductions from the *Burkholderia rhizoxinica* genome. *BMC Genomics* **12,** 210 (2011).
18. Partida-Martinez, L. P. & Hertweck, C. A gene cluster encoding rhizoxin biosynthesis in *Burkholderia rhizoxina*, the bacterial endosymbiont of the fungus *Rhizopus microsporus*. *ChemBioChem* **8,** 41–45 (2007).
19. Kusebauch, B., Busch, B., Scherlach, K., Roth, M. & Hertweck, C. Polyketide-chain branching by an enzymatic Michael addition. *Angew. Chem. Int. Ed. Engl.* **48,** 5001–5004 (2009).
20. Dorrestein, P. C. *et al.* Facile detection of acyl and peptidyl intermediates on thiotemplate carrier domains via phosphopantetheinyl elimination reactions during tandem mass spectrometry. *Biochemistry* **45,** 12756–12766 (2006).
21. Tsai, S.-C. & Ames, B. D. Structural enzymology of polyketide synthases. *Methods Enzymol.* **459,** 17–47 (2009).
22. Maier, T., Leibundgut, M. & Ban, N. The crystal structure of a mammalian fatty acid synthase. *Science* **321,** 1315–1322 (2008).
23. Crawford, J. M. *et al.* Structural basis for biosynthetic programming of fungal aromatic polyketide cyclization. *Nature* **461,** 1139–1143 (2009).
24. Bretschneider, T. *et al.* A ketosynthase homolog uses malonyl units to form esters in cervimycin biosynthesis. *Nature Chem. Biol.* **8,** 154–161 (2011).
25. Fuchs, S. W. *et al.* Formation of 1,3-cyclohexanediones and resorcinols catalyzed by a widely occuring ketosynthase. *Angew. Chem. Int. Ed. Engl.* **52,** 4108–4112 (2013).
26. Piel, J. Biosynthesis of polyketides by *trans*-AT polyketide synthases. *Nat. Prod. Rep.* **27,** 996–1047 (2010).
27. Lim, S. K. *et al. iso*-Migrastatin, migrastatin, and dorrigocin production in *Streptomyces platensis* NRRL 18993 is governed by a single biosynthetic machinery featuring an acyltransferase-less type I polyketide synthase. *J. Biol. Chem.* **284,** 29746–29756 (2009).
28. Wang, B. *et al.* Biosynthesis of 9-methylstreptimidone involves a new decarboxylative step for polyketide terminal diene formation. *Org. Lett.* **15,** 1278–1281 (2013).
29. Rajski, S. R. & Shen, B. Multifaceted modes of action for the glutarimide-containing polyketides revealed. *ChemBioChem* **11,** 1951–1954 (2010).

Supplementary Information is available in the online version of the paper.

Acknowledgements We thank A. Perner for mass specrometry analyses, H. Heineke for NMR measurements, S. Schneider for preliminary studies on the PPTase, and U. Knüpfer for help in protein production. We thank the DFG for financial support (SFB 766) and the Swiss Light Source beamline X06DA for offering beamtime. D.H. is financially supported by a stipend of the Studienstiftung des Deutschen Volkes.

Author Contributions T.B., G.Z. and C.H. designed experiments, T.B., R.W. and B.B. performed genetic and biochemical experiments and analysed data, D.H. and B.K. synthesized substrates and reference compounds, J.B.H., T.S. and G.Z. conducted protein crystallization, X-ray analyses and modelling, T.B., G.Z. and C.H. wrote the manuscript.

Author Information The coordinates and structure factor amplitudes for RhiE* were deposited in the PDB database under accession code 4KC5. Reprints and permissions information is available at www.nature.com/reprints. The authors declare no competing financial interests. Readers are welcome to comment on the online version of the paper. Correspondence and requests for materials should be addressed to C.H. (christian.hertweck@hki-jena.de) and for structural biology to G.Z. (georg.zocher@uni-tuebingen.de).

METHODS

General methods and procedures. MALDI–TOF/TOF measurements were executed with a Bruker UltrafleXtreme device. High-resolution masses were determined using an Exactive mass spectrometer (Thermo Scientific). Protein mass measurement by liquid chromatography/electrospray ionization mass spectrometry (LC-ESI-MS) was accomplished using a ThermoFinnigan Surveyor LC-machine connected to a LTQ velos MS instrument operating with an ESI source. Semi-preparative HPLC was performed on a 1260 Infinity System (Agilent Technologies) equipped with a Zorbax Eclipse XDB-C8 column, 9.5 × 250 mm, particle size: 5 µm (Agilent Technologies). All solvents for analytical and semi-preparative HPLC measurements were obtained commercially at least in gradient grade and were filtered before use. To avoid microbial growth 0.1% formic acid was added to water used for analytical and preparative HPLC. NMR measurements were executed on a Bruker Avance III with cryo probe at resonance frequencies of 600 and 150 MHz for ^{1}H and ^{13}C measurements, respectively. Infrared spectra were recorded on an FT/IR-4100 ATR spectrometer (Jasco). Chemicals were purchased at Sigma-Aldrich and buffer components at Roth.

Cloning procedures. PKS-associated genes were amplified from genomic DNA of *B. rhizoxinica* using *Pfu*-polymerase (Fermentas) with the following primer pairs (used restriction sites are in bold): PPTase-EcoRI-fw (5′-GCTAGC**GAATTC**ATGACCGAGGACGCGACACACATTACG-3′), PPTase-HindIII-rv (5′-GCTAGC**AAGCTT**ACCCGAAGCTGCGGAGGCAATCAAC-3′), ACP-NcoI-fw (5′-**CCATGG**AAAGCAGGAGGCTAAGCCG-3′), ACP-HindIII-rv (5′-**AAGCTT**GACGGAGCTCGAATTCAC-3′), RhiG-SphI-fw (5′-**GCATGC**ATGCCGTACCTCTGCGAAG-3′), RhiG-SphI-rv (5′-**GCATGC**AAACAGGAGTTGACGCGGCTCGG-3′), RhiE*-BamHI-fw (5′-**GGATCC**TCCGGTGAGCGCGTCGAG-3′) and RhiE*-EcoRI-rv (5′-**GAATTC**GGCCATTTCCTATGTCCCAGTCAGTAAGG-3′). The resulting PCR products were cloned into the pCR-Blunt II-TOPO vector (Invitrogen) and subcloned into pHis8-3 (ref. 30) and, in the case of the PPTase gene into pMAL-C2X (NEB), or in the case of RhiG into pQE70. This strategy yielded pSU3, pTB37, pTB39 and pTB57 containing the genes encoding PPTase, ACP, AT (RhiG) and KS-B (RhiE*), respectively. To coexpress the PPTase and ACP genes, pTB37 and pSU3 were restricted with EcoRI and HindIII, and the resulting 839-base-pair (bp) fragment of pSU3 was ligated next to the terminator site of pTB37 to generate pTB40. To warrant expression of both genes, a second ribosome-binding site (RBS) was inserted via two homologous primers. The RBS-1 (5′-P-AATTGA**AGGAGA**TAT-3′) and RBS-2 (5′-P-AATTATA**TCTCCTT**C-3′) (EcoRI site underlined, RBS in bold) primers were annealed together and inserted into EcoRI-restricted pTB40, resulting in pTB41. For production of the standalone B domain (3822-4133, GenBank entry CBW75249.1), the gene region encoding the B domain was amplified by RhiE-B-BamHI-fw (5′-**GGATCC**TCGATCGTCAATCCGCTGATG-3′) and RhiE-B-EcoRI-rv (5′-**GAATTC**GGCCATTTCCTATGTCCCAGTCAGTAAGG-3′). The resulting PCR-product was ligated into pHis, yielding in pTB56. Finally, all expression plasmids were introduced into *Escherichia coli* BL21 (NEB), and, in the case of pTB39, into *E. coli* M15 (Quiagen).

For production of the standalone KS domain two different constructs were designed. First, the region 3152–3661 (GenBank entry CBW75249.1) of the protein sequence was expressed by insertion of a stop codon into pBU191 (RhiE$^{\#}$ in pHis8-3) using the primer pair (stop codon is highlighted in bold) RhiE-A3662STOP-fw (5′-ACCCAGAGCCA**TAG**GACAGCGCCGGACAAATC-3′) and RhiE-A3662STOP-rv (5′-GATTTGTCCGGCGCTGTC**CTA**TGGCTCTGGGT-3′), resulting in pTB49. Second, RhiE-KS with the KS-to-B linker region was expressed from 3152–3837 (GenBank entry CBW75249.1) by insertion of a stop codon into pBU191 using the primer pair (stop codon highlighted in bold) RhiE-A3838STOP-fw (5′-ATCCACTGGTGGCA**TAG**AACTGCTCGACTC-3′) and RhiE-A3838STOP-rv (5′-GAGTCGAGCAGTT**CTA**TGCCACCAGTGGAT-3′), resulting in pTB50.

Protein production. Transformants containing pTB39 were cultivated in LB medium at 27 °C. Immediately after reaching $A_{600\,nm}$ of 0.3–0.5, protein expression was induced by addition of 1 mM isopropyl-β-D-thiogalactopyranoside (IPTG), and cultivation was continued for 15 h.

E. coli transformants containing pSU3, pTB37, pTB41 or pTB57 were cultivated as follows. A 300-ml fermentation broth was inoculated with 30 ml of a pre-culture ($A_{600\,nm}$ = 1.6). After overnight growth, the glucose concentration reached the lower limit and was maintained by addition of 500 mg ml^{-1} glucose solution in a growth rate dependent dosage profile[31]. At $A_{600\,nm} \approx 50$, the protein production was induced by the addition of IPTG to a final concentration of 1 mM. After an additional cultivation of 4 h, the cells were collected by centrifugation at 15,900*g* (Beckman Coulter) at 4 °C for 20 min. The supernatant was removed and the resultant cell pellet was stored at −20 °C.

Protein purification. The histidine-tagged recombinant *apo*/*holo*-ACP, RhiG and KS-B (RhiE$^{\#}$/RhiE*) were purified by similar protocols. In brief, after three cycles of cell disruption for 3 min using a MS73 sonotrode (Bandelin) at 15–20% power the protein lysate (0.1–0.2 g cell pellet per ml buffer) was dissolved in 20 mM Tris buffer, pH 7.5, supplemented with 200 mM NaCl and 50 mM imidazole. The sample was centrifuged, passed through a 0.45-µm filter (Millipore) and loaded onto a 5-ml Protino Ni-NTA column (Macherey-Nagel) connected to an FPLC machine (Äkta Explorer, Amersham Biosciences). Bound proteins were eluted using a 20 mM Tris buffer, pH 7.5, supplemented with 200 mM NaCl and 500 mM imidazole. The resultant fractions were pooled, diluted (1:3) with 20 mM Tris buffer, pH 7.5, and directly loaded onto a 5-ml HiTrap Q HP column (GE Healthcare). Using a gradient of 30 column volumes (0–100%) of a 20 mM Tris buffer, pH 7.5, containing 1 M NaCl the proteins were eluted in this anion-exchange step in a single fraction. Freshly prepared proteins were concentrated using Amicon Ultra-10k or 3-k filters (Millipore) and stored at 4 °C until use or, in case of long-term storage, supplemented with 50% glycerol and frozen at −80 °C. Protein purity and identity of the recombinant proteins was checked by MALDI–TOF/TOF and by PAGE on a 10% SDS gel, or, in case of the ACP, on a 12% SDS gel (Fig. 2B).

***In vitro* phosphopantetheinylation of the ACP.** In a 100-µl reaction scale 10 µM *apo*-ACP were incubated together with 0.2 µM PPTase and 0.25 µM coenzyme A buffered in 100 mM Tris, pH 7.5, containing 12.5 mM $MgCl_2$ and 2.5 mM dithiothreitol. Conversion of *apo*- to *holo*-ACP was monitored by MALDI–TOF. The final recovery of the *holo*-ACP was accomplished by a Ni-NTA column step as described above.

MALDI–TOF/TOF measurements. The MALDI–TOF machine was operated in the positive reflector mode. For control of the biosynthetic reaction acting on the ACP the following settings were used. In the range of 5,000–15,000 Da, 5,000 spectra were recorded with a sampling rate of 1 giga-sample per second using flexControl 3.3 at a laser intensity of 50–90%. Calibration was performed using the protein calibration standard I (Bruker), and subsequent data evaluation was executed in flexAnalysis 3.3. Samples were prepared by mixing of 2 µl sample with 2 µl of 100 µM 2′,5′-dihydroxyacetophenone (contains 2.5 µM diammonium hydrogen citrate) and spotted onto an anchor chip 800/384 T F target (Bruker).

LC-ESI-MS measurements. To analyse malonylated ACP and acylated RhiE$^{\#}$ (RhiE$^{\#}$-Ac) a LC-ESI-MS equipped with a ZORBAX 300SB-CN column (4.6 × 250 mm, 5 µm) was used. The sample components were separated within a gradient of 30–98% solvent B (solvent A: 0.1% HCOOH in water, solvent B: 0.1% HCOOH in acetonitrile) in 26 min with a flow rate of 0.6 ml min^{-1}. The MS-device was used in the positive mode setting.

***In vitro* reconstitution of the branching reaction.** In a 20 mM Tris-buffered (pH 7.0) 40-µl-scale reaction, 3 µM of KS-B was incubated with 166 µM ACP, 0.2 µM RhiG, 730 µM malonyl-CoA and 100 µM (*R*,*S*)-(*E*)-*S*-(2-acetamidoethyl) 5-hydroxyhex-2-enethioate (**2**) at 23 °C with shaking at 400 r.p.m. in a thermomixer (Eppendorf). Analysis of the product formation on the ACP was carried out by MALDI–TOF/TOF as described above.

For mass spectrometry analyses the reaction was terminated by addition of 200 µl ethyl acetate, vortexing and centrifuging. The top organic phase was recovered by pipetting and the volatile ethyl acetate was removed by an upstream flow with nitrogen gas. The resulting pellet was resolved in 60 µl methanol and subjected to HRMS analysis (Exactive).

To decipher the exact reaction mechanism for lactone formation the enzyme assay was performed with ^{13}C-malonyl-CoA in analogy to the procedure described above. However, the reaction conditions needed to be adjusted to warrant stability of the branched reaction product bound to the ACP. Therefore, in this special case, the RhiG enzyme was omitted, as we found that the RhiE ACP domain can be malonylated *in vitro* in the absence of the *trans*-acting acyltransferase RhiG, albeit with a slower production rate. Furthermore, the *holo*-ACP concentration was increased to produce larger amounts of labelled ACP species. In detail, in a 20 mM Tris buffered (pH 7.0) 900-µl-scale reaction, 8 µM of KS-B was incubated with 440 µM ACP, 1.2 mM malonyl-CoA and 1.2 mM (*R*,*S*)-(*E*)-*S*-(2-acetamidoethyl)5-hydroxyhex-2-enethioate (**2**) at 23 °C with shaking at 400 r.p.m. for 48 h in a thermomixer (Eppendorf). The resulting product (**3**) was subsequently purified by size-exclusion chromatography using a HiLoad 16/60 Superdex 200 column (Amersham Bioscience). During the full process the formation and quality of product (**3**) was controlled and analysed by MALDI–TOF. Finally, (**3**) was subjected to NMR measurements with an external reference tube containing tetramethylsilane (TMS).

Mutagenesis of KS-B. RhiE$^{\#}$ mutants were generated using the QuikChange II XL Site-Directed Mutagenesis Kit (Stratagene) and pTB57 as the template. The following primer pairs were used to create the corresponding mutants (mutated triplet is highlighted in bold characters). RhiE-C3228S-fw (5′-TCGATACCATG**TCC**TCGTCGTCCTCGACCTGTA-3′), RhiE-C3228S-rv (5′-TACAGGTCGA**GGA**CGACGAGGACATGGTATCGA-3′), RhiE-C3228A-fw (5′-TATCGATACCATG**GCC**TCGTCGTCCTCGACCTGTA-3′), RhiE-C3228A-rv (5′-TACAGGTCGAGGACGACGA**GGC**CATGGTATCGATA-3′), RhiE-H3364A-fw (5′-C

CTATATCGAGGGC**GCT**GGCTCTGGCACCAAGC-3′), RhiE-H3364A-rv (5′-GCTTGGTGCCAGAGCC**AGC**GCCCTCGATATAGG-3′), RhiE-H3404A-fw (5′-ATCAAGTCGAATATCGGC**GCC**CTATTGGCGGCTTCGG-3′), RhiE-H3404A-rv (5′-CCGAAGCCGCCAATAG**GGC**GCCGATATTCGACTTGAT-3′), RhiE-Y3697F-fw (5′-CTGCTGGATTACGTC**TTC**AGTGGACGG-5′), RhiE-Y3697F-rv (5′-CCG TCCACT**GAA**GACGTAATCCAGCAG-3′), RhiE-D3876A-fw (5′-CCTCGCG ACGACCATT**GCT**AAAGCGCTCTACTTG-3′) and RhiE-D3876A-rv (5′-CAA GTAGAGCGCTTT**AGC**AATGGTCGTCGCGAGG-3′).

Crystallization and structure determination. Initially, we crystallized the native RhiE$^{\#}$ protein including residues 3152–4179 and determined its structure (data not shown). Therefore, we performed crystal screening by sitting drop vapour diffusion at 4 °C and 20 °C using a Freedom Evo system (Tecan) resulting in several crystallization conditions. After several rounds of optimization, plate-like crystals were obtained in crystallization buffer I (15% (w/v) PEG 3350, 190 mM sodium malonate, pH 7.0) by streak seeding. These crystals are of space group $P2_1$ ($a = 125.78$ Å, $b = 145.28$ Å, $c = 131.48$ Å, $\beta = 97.43°$) containing two dimers in the asymmetric unit and had a diffraction limit of 2.7 Å. To evaluate potential structure models as templates for molecular replacement using PHASER[32], the protein sequence was analysed with HHPred[33]. A CHAINSAW[34] and manually modified model of the KS3 domain of module 3 of the 6-deoxyerythronolide B synthase[35] was used as search model. After molecular replacement four-fold NCS-averaging was applied using RESOLVE[36]. The model was improved and completed with several cycles of model building with COOT[37] and refinement using REFMAC5 (ref. 38). The final model comprises three domains, a KS domain, a KS-to-B linker domain, and the B domain (Supplementary Fig. 3), but lacks the first 59 amino acids. Therefore, we decided to use a shorter construct comprising residues 3211–4133 in our follow-up experiments.

RhiE* acylation for substrate cocrystallization. To visualize the polyketide substrate bound to RhiE*, the RhiE* protein fraction eluted from the anion-exchange column (see above) was supplemented with SNAC derivative **2**. In detail, to 5 ml of the pure protein solution (5 mg ml^{-1}), 70 µl of **2** (20 mg ml^{-1}, dissolved in methanol) were added, resulting in a 25-fold excess of the polyketide substrate. After 1 h incubation at 23 °C around 80% of the enzyme molecules were acylated (RhiE*-Ac) as shown by LC-ESI-MS (see above). The acylated protein was subsequently concentrated for size-exclusion chromatography using a Superdex S200/16/60 column equilibrated with SEC-buffer (150 mM NaCl, 20 mM HEPES, pH 7.5).

X-ray structure determination of RhiE*. The truncated and acylated protein was crystallized at 20 °C by mixing the protein solution (5.4 mg ml^{-1}) in a 1:1 ratio with crystallization buffer II (400 nl, 20% (w/v) PEG 2000 MME, 100 mM Tris/HCl, pH 8.5, 100 mM trismethylamine) and placed over the reservoir solution (100 µl crystallization buffer II). Plate-like crystals grew in six weeks to a final size of approximately $200 \times 100 \times 20$ µm^3. Cryo protection was achieved by transferring the crystal into the crystallization buffer II containing glycerol (20% (v/v)) and trismethylamine (200 mM) before flash freezing in liquid nitrogen. The data set of KS-B was recorded at beamline X06DA at the Swiss Light Source in Villigen, Switzerland. Data indexing, integration and scaling were performed with XDS and XSCALE[39]. Crystals of RhiE*-Ac are of the same space group $P2_1$ with slightly different cell dimensions of $a = 125.51$ Å, $b = 144.13$ Å, $c = 131.30$ Å, $\beta = 96.65°$, and diffracted up to 2.14 Å resolution. A rigid body refinement and simulated annealing using PHENIX[40] was used for phasing. The model was completed through several cycles of manual building with COOT, followed by refinement with REFMAC5. Water molecules were placed using COOT:Find_waters. The final refinement step involved TLS parameterization[41] using 1 TLS group per protomer. The geometry of the final model was analysed with MOLPROBITY[42]. Final data statistics are summarized in Supplementary Table 1. Figures were generated using PYMOL[43].

Accession codes. The coordinates and structure factor amplitudes for RhiE* were deposited in the PDB database under accession code 4KC5.

Chemical synthesis and characterization of chemical entities. See Supplementary Information.

30. Jez, J. M., Ferrer, J. L., Bowman, M. E., Dixon, R. A. & Noel, J. P. Dissection of malonyl-coenzyme A decarboxylation from polyketide formation in the reaction mechanism of a plant polyketide synthase. *Biochemistry* **39,** 890–902 (2000).
31. Horn, U. *et al.* High volumetric yields of functional dimeric miniantibodies in *Escherichia coli*, using an optimized expression vector and high-cell-density fermentation under non-limited growth conditions. *Appl. Microbiol. Biotechnol.* **46,** 524–532 (1996).
32. McCoy, A. J. *et al.* Phaser crystallographic software. *J. Appl. Crystallogr.* **40,** 658–674 (2007).
33. Söding, J., Biegert, A. & Lupas, A. N. The HHpred interactive server for protein homology detection and structure prediction. *Nucleic Acids Res.* **33,** W244–W248 (2005).
34. Winn, M. D. *et al.* Overview of the CCP4 suite and current developments. *Acta Crystallogr. D* **67,** 235–242 (2011).
35. Tang, Y., Kim, C. Y., Mathews, I. I., Cane, D. E. & Khosla, C. The 2.7-angstrom crystal structure of a 194-kDa homodimeric fragment of the 6-deoxyerythronolide B synthase. *Proc. Natl Acad. Sci. USA* **103,** 11124–11129 (2006).
36. Terwilliger, T. C. Maximum-likelihood density modification. *Acta Crystallogr. D* **56,** 965–972 (2000).
37. Emsley, P., Lohkamp, B., Scott, W. G. & Cowtan, K. Features and development of Coot. *Acta Crystallogr. D* **66,** 486–501 (2010).
38. Murshudov, G. N. *et al.* REFMAC5 for the refinement of macromolecular crystal structures. *Acta Crystallogr. D* **67,** 355–367 (2011).
39. Kabsch, W. Automatic processing of rotation diffraction data from crystals of initially unknown symmetry and cell constants. *J. Appl. Crystallogr.* **26,** 795–800 (1993).
40. Adams, P. D. *et al.* PHENIX: a comprehensive Python-based system for macromolecular structure solution. *Acta Crystallogr. D* **66,** 213–221 (2010).
41. Winn, M. D., Isupov, M. N. & Murshudov, G. N. Use of TLS parameters to model anisotropic displacements in macromolecular refinement. *Acta Crystallogr. D* **57,** 122–133 (2001).
42. Chen, V. B. *et al.* MolProbity: all-atom structure validation for macromolecular crystallography. *Acta Crystallogr. D* **66,** 12–21 (2010).
43. Schrodinger, L. L. C. The PyMOL Molecular Graphics System, Version 1.5.0.4 (2010).